The RAG1 Ubiquitin Ligase Domain Enhances T Cell Receptor Gene Assembly and Thymic Selection

Thomas N. Burn*[,†,**]; Charline Miot[‡,**]; Portia Kreiger[‡]; Katharina E. Hayer[§]; Anamika Bhattacharyya[¶,‖], Jessica M. Jones[¶], Craig H. Bassing*[,‡,#,††]; Edward M. Behrens*[,†,††]

*Institute for Immunology, Perelman School of Medicine, University of Pennsylvania, Philadelphia, PA 19104
[†]Division of Rheumatology, The Children's Hospital of Philadelphia, Philadelphia, PA 19104
[‡]Department of Pathology and Laboratory Medicine, The Children's Hospital of Philadelphia, Philadelphia, PA 19104
[§]Department of Biomedical and Health Bioinformatics, The Children's Hospital of Philadelphia, Philadelphia, PA 19104
[¶]Department of Biochemistry and Molecular and Cellular Sciences, Georgetown University, Washington, DC, 20057
[‖]Present Address: Vyome Therapeutics Lt., 501 Patparganj Industrial Area, Dehli, India
[#]Department of Pathology and Laboratory Medicine, The Perelman School of Medicine of the University of Pennsylvania, Philadelphia, PA 19104

[**]Co-first Authors

[††]Co-corresponding Authors:
Craig H. Bassing, Ph.D.
Children's Hospital of Philadelphia
4054 Colket Translational Research Building
3501 Civic Center Blvd.
Philadelphia, PA 19104
Phone: 267-426-0311
Email: bassing@email.chop.edu

Edward M. Behrens, M.D.
Children's Hospital of Philadelphia
1102 Abramson Research Center
3615 Civic Center Boulevard
Philadelphia, PA 19104
Phone: 267-426-0142
Email: behrens@email.chop.edu

Abstract

RAG1/RAG2 (RAG) endonuclease-mediated assembly of diverse lymphocyte antigen receptor genes by V(D)J recombination is critical for the development and immune function of T and B cells. However, this process creates highly self-reactive cells that must be negatively selected to suppress autoimmunity. The RAG1 protein contains a ubiquitin ligase domain that stabilizes RAG1 and stimulates RAG endonuclease activity. We report here that mice lacking RAG1 ubiquitin ligase activity exhibit diminished recombination of T cell receptor (TCR) β and α loci, and impaired thymocyte developmental transitions that require the assembly of these genes and signaling by their proteins. The mice also have reduced expression of TCR signaling proteins within thymocytes, less efficient negative selection of highly self-reactive thymocytes, and mature αβ T cells of elevated autoimmune potential. Thus, we propose that the RAG1 ubiquitin ligase domain provides αβ T cell developmental stage-specific means to augment TCR signaling and thereby enhance selection for beneficial TCR genes and against αβ TCRs possessing high autoimmune potential.

Introduction

The ability of T and B lymphocyte populations to express antigen receptors able to recognize a potentially unlimited number of distinct pathogens is the fundamental basis of adaptive immunity. RAG1/RAG2 (RAG) endonuclease-mediated assembly of T cell receptor (TCR) and immunoglobulin (Ig) genes through V(D)J recombination establishes this vast pool of diverse receptors. Germline TCR and Ig loci consist of variable (V), joining (J), and sometimes diversity (D), gene segments residing upstream of constant (C) region exons. During T and B cell development, the lymphocyte-specific RAG complex cooperates with lineage- and developmental stage-specific activation of TCR and Ig loci to perform V(D)J recombination (1). RAG induces DNA double strand breaks (DSBs) between coding sequences and flanking recombination signal sequences of two participating gene segments, liberating hairpin-sealed coding ends and blunt signal ends (2). In a subsequent reaction phase guided by RAG, DNA repair factors ligate signal ends to generate a signal join and open, process, and ligate coding ends to create a V(D)J coding join, which comprises the second exon of an assembled V(D)J-C antigen receptor gene (2). The high number of V(D)J joining events, broad utilization of gene segments, and inherent imprecision in opening and processing coding ends all cooperate to yield a vast population and diversity of receptors. Due to imprecise means of opening and processing coding ends, the outcomes of V(D)J recombination include out-of-frame genes unable to make protein and receptors that recognize self-antigens and have potential for autoimmunity. Accordingly, developing T and B lymphocytes engage quality control checkpoints to select for potentially beneficial antigen receptor proteins and against hazardous highly self-reactive receptors.

Both immature T and B cells employ developmental programs that link functional protein expression from in-frame V(D)J rearrangements to signal either survival and continued differentiation or apoptosis (1). The maturation of αβ T cells in the thymus provides a paradigm for how V(D)J recombination and antigen receptor protein quality control checkpoints cooperate to create a large pool of lymphocytes with diverse

95 receptors that provides immunity from pathogens without causing overt autoimmunity. After entering the
96 thymus, early thymocyte progenitor cells differentiate into $CD44^+CD25^+$ stage 2 and then into $CD44^-$
97 $CD25^+$ stage 3 $CD4^-CD8^-$ double negative (DN) thymocytes (3, 4). Both DN2 and DN3 cells express RAG
98 and conduct V(D)J recombination of *Tcrb*, *Tcrd*, and/or *Tcrg* loci (3, 4). Although DN2-to-DN3
99 thymocyte maturation can occur independent of RAG and V(D)J recombination, an in-frame *Tcrb*
100 rearrangement is necessary for development beyond the DN3 stage (3, 4). The resultant TCRβ protein
101 associates with invariant pTα protein to produce pre-TCR complexes that signal antigen-independent
102 survival, proliferation, and differentiation of DN3 cells (β-selection) into $CD44^-CD25^-$ stage 4 DN
103 thymocytes and then $CD4^+CD8^+$ double-positive (DP) thymocytes (3, 4). DP cells express RAG and
104 conduct V(D)J recombination of *Tcra* loci, which typically proceeds through multiple successive rounds
105 of V-to-J rearrangement on both alleles (5). After an in-frame VJ rearrangement, the resulting TCRα
106 protein can pair with TCRβ protein and yield surface αβ TCRs, which must signal to prevent death by
107 neglect (6-9). This signal activation requires appropriate physical interactions between αβ TCRs and self-
108 peptide/MHC (pMHC) complexes displayed on thymic epithelial cells or dendritic cells, meaning that a
109 functional αβ TCR is inherently self-reactive (6-9). Interactions below a particular low threshold of
110 affinity (or avidity) cannot activate signalling to block apoptosis (6-9). At the other extreme, contacts
111 above a higher threshold trigger strong TCR signalling that causes apoptosis (negative selection) to delete
112 highly self-reactive cells with substantial autoimmune potential (6-9). However, interactions between
113 these two thresholds activate TCR signalling of a strength within a range that promotes survival and
114 differentiation of DP cells (positive selection) into $CD4^+$ or $CD8^+$ single-positive (SP) thymocytes, which
115 lack RAG expression and exit the thymus as mature αβ T cells (6-9). A notable aspect of this αβ TCR
116 quality control checkpoint is that thymocytes are more sensitive than mature αβ T cells as positively-
117 selecting pMHC activates TCR signaling only in the former (9-14). This differential is thought to enable
118 positive selection from low affinity/avidity interactions, prevent the same contacts from activating mature

αβ T cells, and provide a "safety net" for negative selection to more effectively suppress autoimmunity (6-9). Although the T lineage-specific Themis protein contributes to this differential in TCR sensitivity between immature and mature αβ T cells (9, 15, 16), the precise mechanisms by which this protein and possibly additional factors "tune" TCR signaling and control αβ TCR selection remain to be elucidated.

The RAG1 protein N-terminus has a Zinc-binding RING finger E3 ubiquitin ligase domain of undetermined relevance for antigen receptor gene assembly. RAG1 autoubiquitylates on lysine 233 (17), which enhances RAG endonuclease activity as evidenced by impaired cleavage upon mutation of this residue (18). RAG1 also ubiquitylates other proteins including histone H3 within chromatin (19, 20). RAG1 RING domain mutations that disrupt ubiquitin ligase activity impair RAG-mediated cleavage and joining of chromatin substrates, which could be due to loss of histone H3 ubiquitylation and/or alteration in RAG1 protein structure (20-22). The C328Y mutation of a critical structural zinc-binding cysteine of human RAG1 impairs V(D)J recombination and causes severe T and B cell immunodeficiency associated with uncontrolled proliferation of activated oligoclonal αβ T cells (23). The analogous C325Y mutation in mouse Rag1 destabilizes Rag1 tertiary structure, abrogates ubiquitin ligase activity, reduces V(D)J recombination *in vitro*, and causes a near complete block of αβ T cell development at the DN3 thymocyte stage due to impaired *Tcrb* recombination (21, 22). RING domains have a conserved proline (proline 326 in mouse Rag1) that is critical for ubiquitin ligase activity by permitting functional interaction with ubiquitin-conjugating enzymes (24, 25). Relative to C325Y mutation, P326G mutation abrogates RAG1 ubiquitin ligase activity equivalently, but has substantially less severe effects on destabilizing RAG1 protein and reducing RAG endonuclease activity (22). Accordingly, P326 mutation of endogenous mouse RAG1 protein allows an approach to elucidate potential physiologic roles of the RAG1 ubiquitin ligase domain beyond promoting V(D)J recombination by stabilizing RAG1 protein structure.

143 To determine potential *in vivo* functions of RAG1 ubiquitin ligase activity, we created and analyzed mice
144 carrying a homozygous Rag1 P326G mutation. We show that these mice exhibit reduced recombination
145 of *Tcrb* and *Tcra* loci and lower efficiencies of β-selection, positive selection, and negative selection. We
146 find that inactivation of the RAG1 ubiquitin ligase lowers expression of the pre-TCR signaling protein
147 Syk in DN3 thymocytes and of the αβ TCR signaling protein Zap70 in DP thymocytes. Finally, we
148 demonstrate that mature αβ T cells of these mice exhibit normal Zap70 expression and immune responses
149 to activation, yet nevertheless confer greater potential for autoimmunity. Although reduced V(D)J
150 recombination alone could underlie impaired β-selection and positive selection, this does not provide a
151 plausible explanation for less efficient negative selection and greater autoimmunity hazard of αβ T cells.
152 Thus, we propose that the RAG1 ubiquitin ligase domain might provide developmental stage-specific
153 means to increase TCR signaling sensitivities in thymocytes and thereby enhance selection for beneficial
154 *Tcrb* genes and against highly self-reactive αβ TCRs with autoimmune potential.
155

156 **Materials and Methods**
157

158 **Mice**

159 C57BL/6 background *PG* mice were made through gene-targeting as performed by InGenious Targeting
160 Laboratory (2200 Smithtown Avenue, Ronkonkoma, NY). The 9.5 kb genomic DNA used to construct
161 the targeting vector was sub-cloned from a 129Svev BAC clone. The CC>GG double point mutation was
162 shuttled from pJMJ029[P326G](22) into the targeting vector using unique restriction sites, then confirmed
163 by sequencing. Linearized targeting vector was electroporated into BA1 (C57BL/6 x 129/SvEv)
164 embryonic stem (ES) cells. After selection with G418 antibiotic, clones were expanded for PCR analysis
165 to identify recombinant ES clones. Positive clones were screened for short arm integration and then
166 confirmation of the point mutation was performed by PCR and sequencing. Positive clones were analyzed
167 by Southern blot to confirm long arm integration. Injected blastocysts were grown in foster mothers and
168 chimeras were backcrossed against C57BL/6 mice to generate heterozygotes. These were crossed with
169 CMV-*cre* mice (JAX #006054)(26) to remove the *neo* reporter cassette and generate the $Rag1^{P326G}$ allele.
170 After confirmation of *neo* cassette removal, the strain was backcrossed against C57BL/6, and removal of
171 CMV-*cre* was confirmed by PCR. Sequencing of the entire *Rag1* locus in progeny confirmed the intended
172 CC>GG mutation and an additional T>C point mutation that generates a V238A substitution outside of
173 the RING finger domain. The strain was deposited at the Mutant Mouse Regional Resource Center at the
174 University of North Caroline (RAG1-tm1, MMRRC #: 37105). Before initiating studies described herein,
175 the $Rag1^{P326G}$ allele was backcrossed for nine generations onto the C57BL/6 background. To generate
176 NOD background *PG* mice, CRISPR/Cas9-mediated gene editing was conducted in zygotes from *in vitro*
177 fertilization of NOD eggs with NOD sperm. A guide RNA (5'-AAGCACGGATATCGGCAAGA-3') that
178 hybridizes near Rag1 sequences that encode proline 326 was generated as described (27). The following
179 mix was electoporated into zygotes: 4μM of purified guide RNA, 4μM of Cas9-NLS nuclease (qb3
180 MacroLab Berkeley), 10μM of ssDNA 5'-

181 C*A*G*AAAGGACTTCACTGGGCTCTCCAGGTCAGTAGGGAAGCACGGATATCGGCAGGAT
182 CCACAATAGCTGCCCATGACTTTGAGACATCTGAGAATGCAGATCCTACAGAATAGATGCT
183 T-3' (IDT) that contains nucleotides encoding glycine in place of proline at amino acid 326 and a silent
184 point mutation of the next codon which introduce a cleavage site for BamHI restriction enzyme. Mice
185 were screened for introduction of the mutation by PCR with primers 5'-
186 CGTCGCAAGAGAACTCAGGCT-3' and 5'-TCTCGTCAGTGACAGGAGATGCT-3', followed by
187 BamHI digestion of the PCR product. Sanger sequence of PCR products confirmed incorporation of the
188 desired mutation and no other mutations in the *Rag1* coding sequence. Founders with mutations were
189 mated with NOD mice to establish NOD *Rag1*$^{P326G/+}$ mice, which were bred with each other to generate
190 NOD *PG* mice and *WT* littermate controls. NOD mice, C57BL/6 background wild-type and *Rag1*$^{-/-}$ mice
191 and BALB/c background *Rag1*$^{-/-}$ mice were purchased from Jackson Laboratories. All experimental mice
192 were littermates or age-matched with control wild-type animals. All experiments were conducted in
193 accordance with national guidelines and approved by the Institutional Animal Care and Use Committee
194 (IACUC) of the Children's Hospital of Philadelphia.
195
196 **Flow Cytometry**
197 Single cell suspensions of all organs were ACK lysed to remove erythrocytes before being stained with
198 LIVE/DEAD™ Fixable Aqua Dead Cell Stain Kit (Invitrogen) and antibodies against respective surface
199 antigens (BD Biosciences, eBioscience, and Biolegend). Cells were stained for respective intracellular
200 proteins using Cytofix/Cytoperm Fixation/Permeabilization solution kit (BD Biosciences). For staining of
201 intracellular cytokines, cells (1 x10^6) were cultured in the absence or presence of 50 ng/ml PMA (Sigma)
202 and 1μg/ml Ionomycin (Cell Signaling Technology), with 2 μg/ml brefeldin A (Sigma) and 2 μM
203 monensin (eBioscience) for 4 hours at 37°C. After staining for LIVE/DEAD and surface antigens, cells
204 were stained for respective cytokines using the Cytofix/Cytoperm kit (BD Bioscience) or transcription
205 factors using the FoxP3/Transcription Factor staining kit (eBiosciences). Data were acquired on a

206 MACSQuant flow cytometer (Miltenyi Biotec) or LSRII Fortessa (BD Biosciences) and analyzed using
207 Flowjo software version 10.5.3 (Tree Star).
208
209
210 **Cell Sorting**
211 To isolate DN3 cells, thymocytes were stained with PE-labelled CD4, CD8, CD11b, CD11c, NK1.1, Gr1,
212 and Ter119. Non-labelled cells were enriched by MACS depletion using anti-PE microbeads and LS
213 columns (Miltenyi). Enriched cells were then stained with CD4, CD8, CD44, CD25 and anti-lineage/stage
214 markers (TCRβ, B220, CD19, CD11b, CD11c, TCRδ, NK1.1, Ter119) antibodies. DN3 thymocytes were
215 sorted on $Lin^{-}CD4^{-}CD8^{-}CD44^{-}CD25^{+}$ phenotype. To isolate DP cells, thymocytes were stained with CD4,
216 CD8, and anti-lineage (B220, CD19, CD11b, CD11c, TCRδ, NK1.1, Ter119) antibodies. DP thymocytes
217 were sorted on $Lin^{-}CD4^{+}CD8^{+}$ phenotype. The cells of interest were isolated using a FACSAria Fusion
218 sorter (BD Biosciences).
219
220 **Analyzing *Tcrb* and *Tcra* Rearrangements**
221 Genomic DNA was extracted from DN3 or DP cells using the DNeasy Blood and Tissue kit (Qiagen). To
222 measure *Tcrb* rearrangements in DN3 cells, a Taqman PCR assay was used to quantify Vβ-to-DJβ1.1 and
223 Vβ-to-DJβ2.1 rearrangement levels with a primer specific for each Vβ paired and a probe, FAM or HEX,
224 specific for Jβ1.1 or Jβ2.1, respectively. Taqman PCR was performed with conditions according to the
225 manufacturer's instructions (IDT DNA) on the ViiA 7 system (Applied Biosystems). PCR of CD19 was
226 used for normalization. Primers, probes, and reaction conditions are as described (28). To assay *Tcrb*
227 repertoire, DNA from DN3 thymocytes were sent to Adaptive Biotechnologies, who used multiplex PCR
228 to amplify and deep sequence Vβ-Dβ-Jβ rearrangements. Gene segment usage was analyzed by
229 ImmunoSEQ Analyzer software (Adaptive Biotechnologies). To assess *Tcra* rearrangements in DP cells,

230 representative Vα-Jα rearrangements were quantified using a QuantiFast SYBR Green PCR kit (Qiagen)
231 on the ViiA 7 system (Applied Biosystems) as described (29, 30). PCR of β2M was used for normalization.
232

233 **RT-qPCR for mRNA Expression**

234 Respective cell populations were lysed in RLT buffer (Qiagen) containing 2-mercaptoethanol or TRIzol
235 (Life Technologies) immediately after cell sorting. Total RNA was isolated using RNeasy Mini kit
236 (Qiagen), treated with DNase (RNase-Free DNase Set, Qiagen), and reverse transcribed to generate cDNA
237 with High-Capacity RNA-to-cDNA™ Kit (Themo-Fisher Scientific) according to manufacturer's
238 directions. The cDNA was subjected to qPCR using Power SYBR Green kit (Applied Biosystems) and
239 actin, HPRT, ZAP70, and SYK primers (Qiagen). Relative expression was calculated using the ddCt
240 method, using actin or HPRT as a housekeeping gene, and relevant calibrator sample (explained in figure
241 legends for respective samples).
242

243 ***In vitro* T Cell Differentiation**

244 Splenocytes from C57BL/6 background *Rag1*$^{-/-}$ mice were irradiated with 2,500 Rads (X-rad irradiator)
245 and 3 x 10^5 cells were seeded into each well of a 96 well plate. Naïve T cells (CD90.2$^+$, CD4$^+$, CD62L$^+$,
246 CD44$^+$, CD25$^-$) were sorted from C57BL/6 background *WT* or *Rag1*$^{-/-}$ mice using a FACSaria Fusion cell
247 sorter (BD Biosciences), and 3 x 10^4 sorted cells were added to each well containing irradiated feeder
248 cells. All cells were cultured with 10 μg/ml anti-CD3 (Biolegend) and 3 μg/ml anti-CD28 (Biolegend) in
249 RPMI with 10% FBS, 1% PSG, and 1x NEAA (Invitrogen), 1x Sodium Pyruvate (Invitrogen), and 0.001%
250 2-mercaptoethanol. rhIL-2 was used at 30 IU/mL, rmIL-12 and rmIL-4 at 10 ng/mL, rmIL-6 at 20 ng/mL,
251 mTGFβ1 at 1 ng/mL, anti-mIL-4, anti-mIFNγ and anti-mIL-12 at 10 μg/mL (from Biolegend except rhIL-
252 2, rmIL-12, and rmIL-6 from Prepotech). The following cytokines/blocking antibodies were used to skew
253 towards respective Th-subsets: Th0 condition: rhIL-2; Th1 condition: rhIL-2, rmIL-12 and anti-mIL-4;

254 Th2 condition: rhIL-2, rmIL-4, anti-mIFNγ and anti-mIL-12; Th17 condition: rhIL-2, mIL-6, mTGFβ1,
255 anti-mIL-4 and anti-mIL-12; Treg condition: rhIL-2, mTGFβ1, anti-mIL-4 and anti-mIL-12.
256
257 **LCMV Infections**
258 Mice were infected intraperitoneally with 2 x 10^5 plaque-forming units of LCMV-Armstrong and
259 euthanized at indicated timepoints. Virus and gp33-tetramer were kindly provided by E. John Wherry
260 (University of Pennsylvania).
261
262 **T Cell Transfer Model of Colitis**
263 This model was performed as described (31). Briefly, naïve $CD4^+$ T cells were sorted from respective
264 donor mice ($CD90.2^+$, $CD4^+$, $CD62L^+$, $CD44^+$, $CD25^-$) on a FACSAria Fusion cell sorter. 0.5 x 10^6 cells
265 were transferred in 100 μl of PBS into each of the donor mice via intraperitoneal injection. Non-transferred
266 mice were injected with PBS alone. Mice were weighed weekly for the first 4 weeks, and then twice
267 weekly for 4 weeks. Mice were euthanized 8 weeks post-transfer unless severe morbidity enforced
268 premature euthanasia (in accordance with CHOP IACUC approved guidelines) or spontaneous death
269 occurred.
270
271 **Diabetes Onset in NOD Background Mice**
272 NOD background *WT* and *PG* mice were aged and assessed for spontaneous development of diabetes.
273 Mice were aged and monitored for disease to a maximum of 30 weeks of age. Mice older than 10 weeks
274 of age were weekly tested for glycosuria (Uristix®, Siemens). For positive mice, glycosuria was assayed
275 by a second test 24 hours later. Capillary blood glucose of mice testing positive twice for glycosuria was
276 tested via facial vein bleeding. Mice with blood glucose ≥250 mg/dl (13.9 mmol/l) were considered as
277 diabetic and euthanized.
278

279 **Statistical analysis**

280 All data was analyzed in Graphpad Prism 8 using statistical tests indicated in the figure legends. Error
281 bars indicate mean +/- SEM unless otherwise stated. n.s.=$p>0.05$, *$p<0.05$, **$p<0.01$, ***$p<0.001$,
282 ****$p<0.0001$.

283

284 **Results**

285

286

287 **Homozygous Rag1 P326G mutation diminishes TCR gene assembly and subsequent thymocyte**

288 **developmental stage transitions.**

289 To determine potential *in vivo* functions of the RAG1 ubiquitin ligase, we created and analyzed C57BL/6

290 strain mice homozygous for the Rag1 P326G mutation (*Rag1*$^{P326G/P326G}$ mice; see Materials and Methods)

291 that abrogates ubiquitin ligase activity but minimally destabilizes RAG1 protein (22). We initially

292 analyzed αβ T cell development and TCR gene rearrangements in *Rag1*$^{P326G/P326G}$ (*PG*) mice and wild-

293 type (*WT*) mice. As compared to *WT* mice, *PG* mice have a ~2-fold higher percentage and number of DN3

294 thymocytes and correspondingly lower percentage and number of DN4 thymocytes (Fig. 1, A and B). *PG*

295 mice also exhibit ~10% reductions in the percentage and number of DP thymocytes and the ratio of CD4^{+}

296 SP thymocytes to DP thymocytes (Fig. 1, C-E). Despite these minor impairments of the DN-to-DN4 and

297 DP-to-SP thymocyte developmental transitions, *PG* mice have normal numbers of total thymocytes and

298 splenic αβ T cells (Fig. 1 F). We observed ~50% lower levels of rearrangement for nearly all individual

299 Vβ segments in DN3 thymocytes of *PG* mice (Fig. 2, A and B). *Rag1* or *Rag2* mutations that substantially

300 impair RAG endonuclease activity, thymocyte development, and thymic cellularity also alter the usage of

301 individual Vβ segments (32, 33). Yet, reflecting the minor effects of Rag1 P326G mutation, unbiased

302 high-throughput sequencing of *Tcrb* rearrangements in DN3 cells shows similar usage of each Vβ segment

303 in *PG* and *WT* mice (Fig. 2 C). Finally, we detected ~50% lower levels of rearrangements for many of the

304 Vα/Jα combinations assayed in DP thymocytes of *PG* mice (Fig. 2 D). Together, these data show that

305 homozygous Rag1^{P326G} mutation produces RAG endonuclease complexes that catalyze decreased levels

306 of *Tcrb* and *Tcra* rearrangements and support less efficient thymocyte developmental transitions that

307 depend on the functional assembly of a *Tcrb* or *Tcra* gene. Notably, the degrees to which TCR gene

308 rearrangements and αβ T cell development are reduced in *PG* mice are dramatically less than reported for

309 homozygous Rag1 C235Y mutation (21). For example, Rag1^{P236G} mice generate 90% of the normal

310 number of DP thymocytes, whereas homozygous Rag1^{C235Y} mice produce only 1% of the normal number
311 of DP thymocytes. The markedly different severities of these phenotypes indicate that abrogation of RAG1
312 ubiquitin ligase activity without substantial disruption of RAG1 protein structure only slightly impairs
313 V(D)J recombination and αβ T cell development.
314
315 **Inactivation of the RAG1 ubiquitin ligase decreases expression of the signaling proteins Syk and**
316 **Zap70 in thymocytes.**
317 The greater than normal number of DN3 thymocytes in *PG* mice is not typical of a mutation that impairs
318 V(D)J recombination. Instead, this phenotype is consistent with diminished pre-TCR signaling where
319 DN3 cells experiencing β-selection exhibit increased survival but are less efficient than normal at
320 transitioning into DN4 thymocytes. It is notable that thymocytes lacking the Syk pre-TCR signaling
321 protein display this phenotype (34, 35), and that RAG DSBs induced in pre-B cells trigger a genetic
322 program that transcriptionally represses expression of Syk to dampen pre-BCR signaling (36). Thus, we
323 determined whether inactivation of the RAG1 ubiquitin ligase reduces Syk expression in DN3 thymocytes.
324 We detected a slightly lower than normal level of Syk protein in *PG* mice (Fig. 3, A and B); however,
325 unexpectedly, this correlated with an increase in the level of Syk mRNA (Fig. 3 C). These results suggest
326 that RAG DSBs downregulate Syk gene transcription in DN thymocytes, as in pre-B cells, and fewer RAG
327 DSBs from less *Tcrb* recombination in *PG* DN cells leads to higher than normal Syk transcript levels.
328 Despite this, the lower Syk protein expression in *PG* DN thymocytes implies that the RAG1 ubiquitin
329 ligase normally increases translation of Syk mRNA and/or stability of Syk protein during αβ T cell
330 development. Regardless of the underlying mechanisms, these data open the possibility that Syk-mediated
331 pre-TCR signaling is impaired, underlies the accumulation of DN3 thymocytes, and contributes to
332 impaired DN3-to-DN4 thymocyte progression in mice lacking RAG1 ubiquitin ligase activity.
333

334 Given that Syk is related to the Zap70 protein that transduces αβ TCR signals, we determined whether
335 inactivation of the RAG1 ubiquitin ligase also reduces Zap70 expression. To this end, we quantified levels
336 of Zap70 protein and mRNA in DP cells at each of four stages of αβ TCR-signaled positive selection as
337 defined by expression of CD69 and CCR7 proteins (37)(Fig. 3 D). In *PG* mice, we observed lower than
338 normal Zap70 protein levels, but normal levels of TCRβ protein, at each stage of selection (Fig. 3, E-H).
339 We detected normal levels of Zap70 mRNA in cells at each stage assayed in *PG* mice (Fig. 3 I), implying
340 that lower Zap70 mRNA translation and/or Zap70 protein stability is the basis for lower Zap70 expression.
341 RAG DSBs induced during lymphocyte development signal gene expression changes that persist in mature
342 NK cells lacking RAG1 and RAG2 expression (38). We therefore considered whether the Zap70
343 alterations caused by mutant RAG1 during development would also persist in mature T cells after RAG1
344 is no longer expressed. However, we detected normal Zap70 protein levels in splenic $CD4^+$ and $CD8^+$ αβ
345 T cells of *PG* mice (Fig. 3, J and K), indicating that $Rag1^{P326G}$ mutation only reduces Zap70 expression in
346 immature αβ T cells. These data imply that Zap70-mediated □□ TCR signaling might be weaker than
347 normal in developing αβ T cells and thereby contribute to the impaired DP-to-SP thymocyte progression
348 of mice lacking RAG1 ubiquitin ligase activity.
349
350 **Homozygous Rag1 P326G mutation decreases efficiencies of positive and negative selection.**
351 Considering the critical role of Zap70 for positive and negative selection, we investigated whether either
352 of these αβ TCR quality control processes is impaired by the $Rag1^{P326G}$ mutation. As a proxy to establish
353 whether positive selection is impaired in *PG* mice, we determined the frequency of αβ TCR expressing
354 ($TCR\beta^+$) Stage 1 DP thymocytes that initiate positive selection as indicated by progression to Stage 2 in
355 *PG* and *WT* mice (Fig. 4 A). This frequency is lower in *PG* mice (Fig. 4 B). We note that this is an
356 imperfect approach to quantify positive selection because it cannot measure differences in progression

357 through subsequent stages nor cellular fate decisions from specific TCR/pMHC contacts. Nevertheless,
358 our data are consistent with less efficient positive selection in mice lacking RAG1 ubiquitin ligase activity.
359
360 To determine whether the Rag1^{P326G} mutation impairs negative selection, we utilized a naturally occurring
361 system of superantigen-mediated negative selection (39). Laboratory mice express remnant mouse
362 mammary tumor virus (MMTV) retroviral products. Some of these products can bind the MHCII I-E^{d}
363 protein and certain Vβ peptides, including Vβ5.1-5.2 and Vβ12, to trigger exceptionally strong αβ TCR
364 signaling that promotes negative selection (39, 40). BALB/c, but not C57BL/6, strain mice express I-E^{d}
365 protein. As a result, thymocytes expressing Vβ5.1-5.2 or Vβ12 are efficiently deleted in BALB/c, but not
366 B6, genetic backgrounds. We bred BALB/c background *Rag1*$^{-/-}$ mice with C57BL/6 background Rag1 *PG*
367 or *WT* mice to generate and analyze *Rag1*$^{PG/-}$ and *Rag1*$^{WT/-}$ mice expressing I-E^{d} protein. To ascertain
368 whether these mice exhibit a difference in negative selection, we measured frequencies of pre-selected DP
369 thymocytes and post-selection SP thymocytes expressing I-E^{d}:MMTV-reactive (Vβ5^{+} or Vβ12^{+}) or -
370 unreactive (Vβ6^{+}, Vβ8^{+}, or Vβ14^{+}) αβ TCRs (example staining shown in Fig. 4 C). We quantified the
371 fractions of thymocytes expressing each Vβ that progresses through development (are positively selected)
372 and normalized these to the frequencies of total pre- and post-selected cells. For each experiment, we
373 normalized values to the fraction for *Rag1*$^{WT/-}$ mice so that we could combine data from independent
374 experiments (Fig. 4 D). Our analysis indicates that greater fractions of I-E^{d}:MMTV-reactive thymocytes
375 proceed through DP-to-SP development in *Rag1*$^{PG/-}$ mice as compared to *Rag1*$^{WT/-}$ mice (Fig. 4 D),
376 consistent with impaired negative selection of highly self-reactive thymocytes. In contrast, we found that
377 the types of un-reactive thymocytes assayed develop equivalently in each genotype (Fig. 4 D). While the
378 latter finding does not reflect impaired positive selection, we note that this experiment monitors a small
379 subset of thymocytes expressing specific Vβ peptides and thus is not as sensitive as determining the

380 frequencies of DP cells that initiate positive selection. Regardless, we conclude that inactivation of the
381 RAG1 ubiquitin ligase renders negative selection less efficient.
382
383 **Mature αβ T cells that develop without RAG1 ubiquitin ligase activity exhibit normal responses to**
384 **activation.**
385 RAG endonuclease activity during lymphocyte ontogeny triggers permanent changes in gene expression
386 that correlate with impaired immune responses of mature lymphocytes (38). Although we did not observe
387 any differences in Zap70 protein levels between splenic αβ T cells of *PG* and *WT* mice, we sought to
388 elucidate whether mature αβ T cells that develop without RAG1 ubiquitin ligase activity have normal or
389 altered response to activation. We first conducted *in vitro* analyses. Upon stimulation with PMA and
390 ionomycin, splenic $CD44^{hi}$ αβ T cells from *PG* mice produce normal levels of IFNγ, TNFα, IL-2, and IL-
391 17A (Fig. 5 A). These cells also show normal proliferation upon anti-CD3/anti-CD28 stimulation (Fig. 5
392 B). Moreover, stimulated $CD4^+$ and $CD8^+$ αβ T cells of *PG* mice normally express their canonical
393 transcription factors (Fig. 5, C and D) and cytokines (Fig. 5, E and F) when cultured in respective skewing
394 conditions. We next monitored αβ T cell responses *in vivo* following infection of mice with an acute strain
395 of lymphocytic choriomeningitis virus (LCMV-Armstrong). We analyzed mice either seven days later to
396 monitor at the immune response peak or 35 days later to monitor memory cells. At each timepoint, we
397 detected similar frequencies and numbers of antigen-specific $CD8^+$ αβ T cells that stain with gp33:H-2Db
398 tetramer in *PG* and *WT* mice (Fig. 5 G), indicating that *PG* mice display normal numbers and dynamic
399 responses of αβ T cells that recognize LCMV-Armstrong. We also observed equivalent dynamic
400 expression of Tbet, Eomes, KLRG1, and CD127 proteins on αβ T cells from *PG* and *WT* mice (Fig. 5 H),
401 indicating normal contraction of short-lived effector cells (SLECs), and sustained memory/memory
402 precursor effector cells (MPECs) in *PG* mice. Finally, we detected similar numbers of antigen specific αβ
403 T cells able to respond to the gp33, NP396, or gp61 viral peptides within a peptide re-stimulation assay

404 (Fig. 5, I and J). Together, these data support the notion that the development of αβ T cells in the absence
405 of RAG1 ubiquitin ligase activity does not substantially alter responses of these mature immune cells to
406 activation.
407
408 **Mature αβ T cells that develop in the absence of RAG1 ubiquitin ligase activity exhibit increased**
409 **predisposition to autoimmunity.**
410 In a setting of less efficient negative selection as with homozygous $Rag1^{P326G}$ mutation, an increased
411 predisposition to αβ T cell mediated autoimmunity would be expected. However, we have not observed
412 overt autoimmune symptoms within *PG* mice, possibly because mice of the C57BL/6 background are
413 resistant to spontaneous autoimmune diseases (41, 42). Thus, to investigate whether the $Rag1^{P326G}$
414 mutation can predispose to autoimmunity, we utilized an induced model of autoimmune colitis in
415 C57BL/6 mice and a spontaneous model of autoimmune diabetes in NOD mice.
416
417 The colitis model involves transferring into *Rag1*$^{-/-}$ mice naïve $CD4^+$ effector αβ T cells, which become
418 activated and trigger cytokine-driven colitis and associated systemic pathologies including weight loss
419 due to the absence of Tregs (31, 43, 44). We observed accelerated wasting of *Rag1*$^{-/-}$ mice receiving *PG*
420 cells relative to *WT* cells or no transfer (Fig. 6 A). We analyzed mice at eight weeks after transfer. As
421 compared to *WT* recipients, we detected greater numbers of total splenic $CD4^+$ T cells and of $CD4^+$ T cells
422 producing IFNγ, TNFα, and/or GM-CSF cytokines (Fig. 6, B and C). Colon length is used as a measure
423 of disease severity in this model, and mice receiving transferred *PG* cells had shorter colons relative to
424 mice receiving *WT* cells, consistent with worse disease caused by *PG* cells (Fig. 6 D). Histologic
425 assessment and scoring in this colitis model has been formalized (44), and can be grossly broken down
426 into scores related to inflammatory cell infiltration and scores related to injury of tissue architecture. There
427 was no statistical difference in inflammation scores between mice receiving *WT* and *PG* cells. However,

428 tissue damage scores were higher in mice receiving *PG* cells, suggesting that, on a per cell basis, *PG* cells
429 induce greater tissue injury in this model (Fig. 6, E-F). Notably, specifically in *PG*-transferred animals,
430 we observed autoimmune pathologies in addition to colitis, including dermatitis, chylous ascites, severe
431 small intestine enlargement, and neurological stress (Fig. 6 H). Dermatitis was most common and involved
432 massive inflammatory infiltration and tissue damage (Fig. 6 I). Consistent with more widespread
433 autoimmune conditions in *PG*-transferred mice, we significant splenomegaly in these mice (Fig. 6 J).
434 Finally, while not statistically significant, we observed an increased rate of premature death in the mice
435 transferred with *PG* cells compared to *WT* cells (Fig. 6K), which was especially surprising because death
436 is an unexpected outcome in this model. Collectively, the data from this colitis model indicate that $CD4^+$
437 effector T cells from *PG* mice have greater than normal intrinsic autoimmune potential.
438
439 To determine whether inactivation of the Rag1 ubiquitin ligase enhances autoimmunity in another genetic
440 background, we utilized CRISPR/Cas9-mediated gene editing to establish NOD mice with the $Rag1^{P326G}$
441 mutation. NOD mice develop spontaneous αβ T cell driven diabetes at an incidence of 60–80% in females
442 and 20–30% in males (45, 46). We bred together NOD:$Rag1^{P326G/WT}$ mice to create cohorts of NOD *PG*
443 and *WT* females, which we aged and screened for diabetes by monitoring glycosuria and blood glucose
444 levels. We observed accelerated onset of diabetes in *PG* mice compared to *WT* mice (Fig. 6 L).
445 Collectively, our analyses of the colitis and diabetes models on mice of two different genetic backgrounds
446 indicate that homozygous $Rag1^{P326G}$ mutation increases predisposition to αβ T cell mediated
447 autoimmunity.
448
449
450

451 **Discussion**

452

453 Our analysis of homozygous Rag1^{P326G} mice reveals roles for the RAG1 RING domain ubiquitin ligase in
454 stimulating TCR gene assembly, shaping thymocyte gene expression, and enhancing TCR quality control
455 checkpoints. As expected from *in vitro* analyses, the Rag1^{P326G} mutant produces RAG endonuclease
456 complexes that catalyze modestly decreased V(D)J recombination of *Tcrb* and *Tcra* loci in thymocytes.
457 While a less efficient RAG endonuclease could account entirely for the reduced assembly of *Tcrb* and
458 *Tcra* genes, additional experiments are necessary to investigate potential functions of the RAG1 ubiquitin
459 ligase in modulating chromatin accessibility and/or RAG binding of these loci. The reduced assembly of
460 *Tcrb* genes most likely contributes to the impaired DN3-to-DN4 thymocyte development of *PG* mice, as
461 is the case in mice homozygous for other *Rag1* or *Rag2* mutations that lower RAG endonuclease activity
462 (21, 33). To our knowledge, reduced V(D)J recombinase function has not been demonstrated to increase
463 DN3 thymocyte numbers; however, Syk inactivation has because it impairs pre-TCR signals that drive
464 differentiation of DN3 cells (34, 35). Accordingly, it is plausible that reduced Syk protein expression in
465 DN3 thymocytes contributes to their accumulation in *PG* mice, highlighting a potential role of the RAG1
466 ubiquitin ligase in promoting early thymocyte development beyond stimulating *Tcrb* gene assembly. Yet,
467 unequivocal conclusions require elucidating how Rag1^{P326G} mutation impairs Syk expression and
468 specifically disrupting these mechanisms.

469

470 We next considered effects of Rag1 RING domain ubiquitin ligase inactivation on the DP-to-SP
471 thymocyte developmental transition. Given that deletion of most Jα segments in mice impairs DP-to-SP
472 thymocyte development due to fewer chances for each DP cell to produce a positively-selected TCR (47),
473 it is possible that reduced *Tcra* recombination contributes to less efficient positive selection in *PG* mice.
474 Accordingly, we cannot definitively attribute a non-V(D)J recombination effect of Rag1 ubiquitin ligase
475 inactivation to positive selection. In contrast, our data indeed support a non-V(D)J recombination effect

476 of reduced Rag1 ubiquitin ligase activity on negative selection. In DP thymocytes with normal V(D)J
477 recombinase function, the expression of a highly self-reactive αβ TCR signals apoptosis before ongoing
478 *Tcra* recombination can generate a new αβ TCR (48). Consequently, it is hard to conceive how reduced
479 RAG endonuclease activity would impair negative selection. However, as reduced Zap70 activity impairs
480 αβ TCR signaling and negative selection (49-51), attenuated αβ TCR signaling from lower Zap70 protein
481 expression is a plausible explanation for less efficient superantigen-mediated negative selection in *PG*
482 mice. However, definitive conclusions necessitate determining how Rag1^{P326G} mutation impairs Zap70
483 expression and specifically disrupting these mechanisms.
484
485 Based on our findings, we propose that RAG1 ubiquitin ligase activity upregulates expression of Syk and
486 Zap70 protein respectively, to enhance β-selection of positive and negative selection of thymocytes. We
487 acknowledge that Syk and Zap70 protein levels are only slightly lower than normal in *PG* mice and that
488 we have not proven that these differences underlie impaired β-selection, positive selection, and negative
489 selection. We did not observe differences in Syk or Zap70 activation or other aspects of TCR signaling
490 between *WT* and *PG* thymocytes following anti-CD3 stimulation (data not shown). However, this methods
491 of activating TCR signaling is not as sensitive for detecting differences as using MHC to present different
492 peptides to a fixed transgenic αβ TCR (9, 10, 16), which is beyond the scope of this study. Moreover, we
493 note that small reductions in Zap70 activity render negative selection less efficient (49-51). In addition,
494 we consider it likely that Rag1^{P326G} mutation also might alter expression of other proteins, with the
495 cumulative changes having synergistic effects on TCR signaling and thymocyte selection. To rigorously
496 test our model, it will be necessary to elucidate the extent and mechanisms by which the RAG1 ubiquitin
497 ligase modulates gene expression, and then disrupt these pathways, preferably without also reducing RAG
498 endonuclease activity. Likewise, it will be important to determine whether Rag1^{P326G} mutation has any
499 effects on the thymic microenvironment (i.e. defective maturation of thymic epithelial cells and/or

500 distribution of dendritic cells) as is observed in mouse models with impaired V(D)J recombination and a
501 resulting dramatically reduced thymic cellularity (52). However, unlike these models, *PG* mice have
502 relatively normal numbers of thymocytes, which should facilitate distinction of thymocyte intrinsic versus
503 extrinsic effects on αβ TCR selection.
504
505 There are multiple not mutually exclusive mechanisms by which the RAG1 ubiquitin ligase domain could
506 increase Syk and Zap70 protein levels within thymocytes. In pre-B cells, RAG DSBs signal transcriptional
507 activation of a broad multifunctional genetic program, with one component being decreased Syk protein
508 expression to attenuate pre-BCR signaling and facilitate assembly of Ig light chain genes (36, 53). RAG
509 DSBs in thymocytes could trigger transcriptional and post-transcriptional up-regulation of Syk and Zap70
510 expression, where fewer RAG DSBs from $Rag1^{P326G}$ mutation specifically impairs post-transcriptional
511 mechanisms. DSB-induced covalent modifications of histones in chromatin around breakage sites are
512 critical for amplifying DNA damage response (54). The inability of $Rag1^{P326G}$ to ubiquitylate histone H3
513 and other potential target proteins at RAG DSBs might dampen or prevent signals that mediate post-
514 transcriptional upregulation of Syk and Zap70. Alternatively, the RAG1 ubiquitin ligase domain might
515 elevate Syk and Zap70 protein expression independent of RAG endonuclease activity, such as by binding
516 and/or ubiquitylating factors that regulate translation or turnover of these TCR signaling proteins.
517 Whatever mechanisms an intact RAG1 ubiquitin ligase domain employs to stimulate Syk and Zap70
518 protein expression, their effects would be temporary and terminated after cessation of RAG1 expression
519 following positive selection as evidenced by normal Zap70 protein levels in mature αβ T cells as well as
520 their normal function to infectious challenges.
521
522 The requirement for αβ TCR selection on pMHC presents major challenges for establishing an αβ T cell
523 population that recognizes and responds to diverse foreign peptides, but not self-peptides. An inability to
524 positively-select αβ TCRs with very low affinity/avidity for pMHC could eliminate T cells capable of

525 binding foreign peptides with no similarities to self-peptides, generating holes in adaptive immunity. At
526 the same time, any positively-selected TCR is able to recognize a self-peptide and thus could cause
527 autoimmunity. To meet these challenges, cell intrinsic mechanisms have evolved to render thymocytes
528 more sensitive to TCR stimulation than their mature αβ T cell counterparts (10-14). This "TCR signal
529 tuning" elevates the affinity/avidity thresholds for both positive and negative selection because any
530 functional TCR/pMHC interaction triggers a stronger TCR signal in thymocytes versus αβ T cells (6-9).
531 This lower sensitivity of mature αβ T cells prevents their activation when encountering an pMHC identical
532 to that on which they were positively-selected. Although several factors have been implicated in regulating
533 TCR signal tuning, each is expressed in both thymocytes and mature αβ T cells (16, 55-59). Our
534 observations of reduced thymic Zap70 expression and less efficient positive and negative selection in *PG*
535 mice suggest that the RAG1 protein might serve as a "TCR signal tuning" factor. The thymocyte specific
536 developmental timing of RAG1 expression makes it an excellent candidate to serve as one such tuning
537 factor. In this scenario, the ability of the RAG1 ubiquitin ligase domain to upregulate Zap70, and perhaps
538 modulate expression of additional factors, would raise TCR/pMHC affinity/avidity thresholds for positive
539 selection and negative selection. Therefore, we propose that the RAG1 ubiquitin ligase domain provides
540 developmental stage-specific means to stimulate positive selection of potentially beneficial TCRs and
541 negative selection of highly self-reactive TCRs with greatest autoimmune potential. Critically, our study
542 provides a phenotypic framework from which to elucidate the exact molecular mechanisms by which the
543 RAG1 ubiquitin ligase promotes TCR gene assembly and transcends this process to govern the proper
544 selection of developing αβ T cells.
545
546
547

548 **Acknowledgements**

549 We thank Kyutae Lee for designing the gene-editing strategy and Adele Harman of the CHOP Transgenic
550 Core to generate the NOD *PG* mice. The authors have no completing financial interests to declare.

551

552

553

554

555

556 **References**
557

558 1. Bassing, C. H., W. Swat, and F. W. Alt. 2002. The mechanism and regulation of chromosomal
559 V(D)J recombination. *Cell* 109 Suppl: S45-55.
560 2. Schatz, D. G., and P. C. Swanson. 2011. V(D)J recombination: mechanisms of initiation. *Annu*
561 *Rev Genet* 45: 167-202.
562 3. Bhandoola, A., H. von Boehmer, H. T. Petrie, and J. C. Zuniga-Pflucker. 2007. Commitment and
563 developmental potential of extrathymic and intrathymic T cell precursors: plenty to choose from.
564 *Immunity* 26: 678-689.
565 4. von Boehmer, H., and F. Melchers. 2010. Checkpoints in lymphocyte development and
566 autoimmune disease. *Nat Immunol* 11: 14-20.
567 5. Carico, Z., and M. S. Krangel. 2015. Chromatin Dynamics and the Development of the TCRalpha
568 and TCRdelta Repertoires. *Adv Immunol* 128: 307-361.
569 6. Hogquist, K. A., and S. C. Jameson. 2014. The self-obsession of T cells: how TCR signaling
570 thresholds affect fate 'decisions' and effector function. *Nat Immunol* 15: 815-823.
571 7. Gascoigne, N. R., V. Rybakin, O. Acuto, and J. Brzostek. 2016. TCR Signal Strength and T Cell
572 Development. *Annu Rev Cell Dev Biol* 32: 327-348.
573 8. Klein, L., B. Kyewski, P. M. Allen, and K. A. Hogquist. 2014. Positive and negative selection of
574 the T cell repertoire: what thymocytes see (and don't see). *Nat Rev Immunol* 14: 377-391.
575 9. Fu, G., V. Rybakin, J. Brzostek, W. Paster, O. Acuto, and N. R. Gascoigne. 2014. Fine-tuning T
576 cell receptor signaling to control T cell development. *Trends Immunol* 35: 311-318.
577 10. Davey, G. M., S. L. Schober, B. T. Endrizzi, A. K. Dutcher, S. C. Jameson, and K. A. Hogquist.
578 1998. Preselection thymocytes are more sensitive to T cell receptor stimulation than mature T cells.
579 *J Exp Med* 188: 1867-1874.
580 11. Lucas, B., I. Stefanova, K. Yasutomo, N. Dautigny, and R. N. Germain. 1999. Divergent changes
581 in the sensitivity of maturing T cells to structurally related ligands underlies formation of a useful
582 T cell repertoire. *Immunity* 10: 367-376.
583 12. Yachi, P. P., C. Lotz, J. Ampudia, and N. R. Gascoigne. 2007. T cell activation enhancement by
584 endogenous pMHC acts for both weak and strong agonists but varies with differentiation state. *J*
585 *Exp Med* 204: 2747-2757.
586 13. Pircher, H., U. H. Rohrer, D. Moskophidis, R. M. Zinkernagel, and H. Hengartner. 1991. Lower
587 receptor avidity required for thymic clonal deletion than for effector T-cell function. *Nature* 351:
588 482-485.
589 14. Sant'Angelo, D. B., and C. A. Janeway, Jr. 2002. Negative selection of thymocytes expressing the
590 D10 TCR. *Proc Natl Acad Sci U S A* 99: 6931-6936.
591 15. Choi, S., R. Cornall, R. Lesourne, and P. E. Love. 2017. THEMIS: Two Models, Different
592 Thresholds. *Trends Immunol* 38: 622-632.
593 16. Fu, G., J. Casas, S. Rigaud, V. Rybakin, F. Lambolez, J. Brzostek, J. A. Hoerter, W. Paster, O.
594 Acuto, H. Cheroutre, K. Sauer, and N. R. Gascoigne. 2013. Themis sets the signal threshold for
595 positive and negative selection in T-cell development. *Nature* 504: 441-445.
596 17. Jones, J. M., and M. Gellert. 2003. Autoubiquitylation of the V(D)J recombinase protein RAG1.
597 *Proc Natl Acad Sci U S A* 100: 15446-15451.
598 18. Singh, S. K., and M. Gellert. 2015. Role of RAG1 autoubiquitination in V(D)J recombination.
599 *Proc Natl Acad Sci U S A* 112: 8579-8583.
600 19. Jones, J. M., A. Bhattacharyya, C. Simkus, B. Vallieres, T. D. Veenstra, and M. Zhou. 2011. The
601 RAG1 V(D)J recombinase/ubiquitin ligase promotes ubiquitylation of acetylated, phosphorylated
602 histone 3.3. *Immunol Lett* 136: 156-162.

603 20. Grazini, U., F. Zanardi, E. Citterio, S. Casola, C. R. Goding, and F. McBlane. 2010. The RING
604 domain of RAG1 ubiquitylates histone H3: a novel activity in chromatin-mediated regulation of
605 V(D)J joining. *Mol Cell* 37: 282-293.
606 21. Deng, Z., H. Liu, and X. Liu. 2015. RAG1-mediated ubiquitylation of histone H3 is required for
607 chromosomal V(D)J recombination. *Cell Res* 25: 181-192.
608 22. Simkus, C., P. Anand, A. Bhattacharyya, and J. M. Jones. 2007. Biochemical and folding defects
609 in a RAG1 variant associated with Omenn syndrome. *J Immunol* 179: 8332-8340.
610 23. Villa, A., C. Sobacchi, L. D. Notarangelo, F. Bozzi, M. Abinun, T. G. Abrahamsen, P. D.
611 Arkwright, M. Baniyash, E. G. Brooks, M. E. Conley, P. Cortes, M. Duse, A. Fasth, A. M.
612 Filipovich, A. J. Infante, A. Jones, E. Mazzolari, S. M. Muller, S. Pasic, G. Rechavi, M. G. Sacco,
613 S. Santagata, M. L. Schroeder, R. Seger, D. Strina, A. Ugazio, J. Valiaho, M. Vihinen, L. B. Vogler,
614 H. Ochs, P. Vezzoni, W. Friedrich, and K. Schwarz. 2001. V(D)J recombination defects in
615 lymphocytes due to RAG mutations: severe immunodeficiency with a spectrum of clinical
616 presentations. *Blood* 97: 81-88.
617 24. Zheng, N., P. Wang, P. D. Jeffrey, and N. P. Pavletich. 2000. Structure of a c-Cbl-UbcH7 complex:
618 RING domain function in ubiquitin-protein ligases. *Cell* 102: 533-539.
619 25. Albert, T. K., H. Hanzawa, Y. I. Legtenberg, M. J. de Ruwe, F. A. van den Heuvel, M. A. Collart,
620 R. Boelens, and H. T. Timmers. 2002. Identification of a ubiquitin-protein ligase subunit within
621 the CCR4-NOT transcription repressor complex. *EMBO J* 21: 355-364.
622 26. Schwenk, F., U. Baron, and K. Rajewsky. 1995. A cre-transgenic mouse strain for the ubiquitous
623 deletion of loxP-flanked gene segments including deletion in germ cells. *Nucleic Acids Res* 23:
624 5080-5081.
625 27. Lee, K. D., and C. H. Bassing. 2020. Two Successive Inversional Vbeta Rearrangements on a
626 Single Tcrb Allele Can Contribute to the TCRbeta Repertoire. *J Immunol* 204: 78-86.
627 28. Gopalakrishnan, S., K. Majumder, A. Predeus, Y. Huang, O. I. Koues, J. Verma-Gaur, S.
628 Loguercio, A. I. Su, A. J. Feeney, M. N. Artyomov, and E. M. Oltz. 2013. Unifying model for
629 molecular determinants of the preselection Vbeta repertoire. *Proc Natl Acad Sci U S A* 110: E3206-
630 3215.
631 29. Shih, H. Y., J. Verma-Gaur, A. Torkamani, A. J. Feeney, N. Galjart, and M. S. Krangel. 2012.
632 Tcra gene recombination is supported by a Tcra enhancer- and CTCF-dependent chromatin hub.
633 *Proc Natl Acad Sci U S A* 109: E3493-3502.
634 30. Chen, L., Z. Carico, H. Y. Shih, and M. S. Krangel. 2015. A discrete chromatin loop in the mouse
635 Tcra-Tcrd locus shapes the TCRdelta and TCRalpha repertoires. *Nat Immunol* 16: 1085-1093.
636 31. Ostanin, D. V., J. Bao, I. Koboziev, L. Gray, S. A. Robinson-Jackson, M. Kosloski-Davidson, V.
637 H. Price, and M. B. Grisham. 2009. T cell transfer model of chronic colitis: concepts,
638 considerations, and tricks of the trade. *Am J Physiol Gastrointest Liver Physiol* 296: G135-146.
639 32. Liang, H. E., L. Y. Hsu, D. Cado, L. G. Cowell, G. Kelsoe, and M. S. Schlissel. 2002. The
640 "dispensable" portion of RAG2 is necessary for efficient V-to-DJ rearrangement during B and T
641 cell development. *Immunity* 17: 639-651.
642 33. Horowitz, J. E., and C. H. Bassing. 2014. Noncore RAG1 regions promote Vbeta rearrangements
643 and alphabeta T cell development by overcoming inherent inefficiency of Vbeta recombination
644 signal sequences. *J Immunol* 192: 1609-1619.
645 34. Colucci, F., D. Guy-Grand, A. Wilson, M. Turner, E. Schweighoffer, V. L. Tybulewicz, and J. P.
646 Di Santo. 2000. A new look at Syk in alpha beta and gamma delta T cell development using
647 chimeric mice with a low competitive hematopoietic environment. *J Immunol* 164: 5140-5145.
648 35. Palacios, E. H., and A. Weiss. 2007. Distinct roles for Syk and ZAP-70 during early thymocyte
649 development. *J Exp Med* 204: 1703-1715.
650 36. Bednarski, J. J., R. Pandey, E. Schulte, L. S. White, B. R. Chen, G. J. Sandoval, M. Kohyama, M.
651 Haldar, A. Nickless, A. Trott, G. Cheng, K. M. Murphy, C. H. Bassing, J. E. Payton, and B. P.

652 Sleckman. 2016. RAG-mediated DNA double-strand breaks activate a cell type-specific
653 checkpoint to inhibit pre-B cell receptor signals. *J Exp Med* 213: 209-223.
654 37. Kimura, M. Y., J. Thomas, X. Tai, T. I. Guinter, M. Shinzawa, R. Etzensperger, Z. Li, P. Love, T.
655 Nakayama, and A. Singer. 2016. Timing and duration of MHC I positive selection signals are
656 adjusted in the thymus to prevent lineage errors. *Nat Immunol* 17: 1415-1423.
657 38. Karo, J. M., D. G. Schatz, and J. C. Sun. 2014. The RAG recombinase dictates functional
658 heterogeneity and cellular fitness in natural killer cells. *Cell* 159: 94-107.
659 39. Jordan, M. S., J. E. Smith, J. C. Burns, J. E. Austin, K. E. Nichols, A. C. Aschenbrenner, and G.
660 A. Koretzky. 2008. Complementation in trans of altered thymocyte development in mice
661 expressing mutant forms of the adaptor molecule SLP76. *Immunity* 28: 359-369.
662 40. Surh, C. D., and J. Sprent. 1994. T-cell apoptosis detected in situ during positive and negative
663 selection in the thymus. *Nature* 372: 100-103.
664 41. Jiang, W., M. S. Anderson, R. Bronson, D. Mathis, and C. Benoist. 2005. Modifier loci condition
665 autoimmunity provoked by Aire deficiency. *J Exp Med* 202: 805-815.
666 42. Jin, Y., A. Lee, J. H. Oh, H. W. Lee, and S. J. Ha. 2019. The R229Q mutation of Rag2 does not
667 characterize severe immunodeficiency in mice. *Sci Rep* 9: 4415.
668 43. Mottet, C., H. H. Uhlig, and F. Powrie. 2003. Cutting edge: cure of colitis by CD4+CD25+
669 regulatory T cells. *J Immunol* 170: 3939-3943.
670 44. Eri, R., M. A. McGuckin, and R. Wadley. 2012. T cell transfer model of colitis: a great tool to
671 assess the contribution of T cells in chronic intestinal inflammation. *Methods Mol Biol* 844: 261-
672 275.
673 45. Anderson, M. S., and J. A. Bluestone. 2005. The NOD mouse: a model of immune dysregulation.
674 *Annu Rev Immunol* 23: 447-485.
675 46. Delovitch, T. L., and B. Singh. 1997. The nonobese diabetic mouse as a model of autoimmune
676 diabetes: immune dysregulation gets the NOD. *Immunity* 7: 727-738.
677 47. Huang, C. Y., B. P. Sleckman, and O. Kanagawa. 2005. Revision of T cell receptor {alpha} chain
678 genes is required for normal T lymphocyte development. *Proc Natl Acad Sci U S A* 102: 14356-
679 14361.
680 48. Kreslavsky, T., H. J. Kim, S. B. Koralov, D. Ghitza, T. Buch, H. Cantor, K. Rajewsky, and H. von
681 Boehmer. 2013. Negative selection, not receptor editing, is a physiological response of
682 autoreactive thymocytes. *J Exp Med* 210: 1911-1918.
683 49. Sakaguchi, N., T. Takahashi, H. Hata, T. Nomura, T. Tagami, S. Yamazaki, T. Sakihama, T.
684 Matsutani, I. Negishi, S. Nakatsuru, and S. Sakaguchi. 2003. Altered thymic T-cell selection due
685 to a mutation of the ZAP-70 gene causes autoimmune arthritis in mice. *Nature* 426: 454-460.
686 50. Mallaun, M., G. Zenke, and E. Palmer. 2010. A discrete affinity-driven elevation of ZAP-70 kinase
687 activity initiates negative selection. *J Recept Signal Transduct Res* 30: 430-443.
688 51. Hsu, L. Y., Y. X. Tan, Z. Xiao, M. Malissen, and A. Weiss. 2009. A hypomorphic allele of ZAP-
689 70 reveals a distinct thymic threshold for autoimmune disease versus autoimmune reactivity. *J Exp*
690 *Med* 206: 2527-2541.
691 52. Marrella, V., P. L. Poliani, L. D. Notarangelo, F. Grassi, and A. Villa. 2014. Rag defects and
692 thymic stroma: lessons from animal models. *Front Immunol* 5: 259.
693 53. Bredemeyer, A. L., B. A. Helmink, C. L. Innes, B. Calderon, L. M. McGinnis, G. K. Mahowald,
694 E. J. Gapud, L. M. Walker, J. B. Collins, B. K. Weaver, L. Mandik-Nayak, R. D. Schreiber, P. M.
695 Allen, M. J. May, R. S. Paules, C. H. Bassing, and B. P. Sleckman. 2008. DNA double-strand
696 breaks activate a multi-functional genetic program in developing lymphocytes. *Nature* 456: 819-
697 823.
698 54. Van, H. T., and M. A. Santos. 2018. Histone modifications and the DNA double-strand break
699 response. *Cell Cycle* 17: 2399-2410.

700 55. Fu, G., S. Vallee, V. Rybakin, M. V. McGuire, J. Ampudia, C. Brockmeyer, M. Salek, P. R. Fallen,
701 J. A. Hoerter, A. Munshi, Y. H. Huang, J. Hu, H. S. Fox, K. Sauer, O. Acuto, and N. R. Gascoigne.
702 2009. Themis controls thymocyte selection through regulation of T cell antigen receptor-mediated
703 signaling. *Nat Immunol* 10: 848-856.
704 56. Lesourne, R., S. Uehara, J. Lee, K. D. Song, L. Li, J. Pinkhasov, Y. Zhang, N. P. Weng, K. F.
705 Wildt, L. Wang, R. Bosselut, and P. E. Love. 2009. Themis, a T cell-specific protein important for
706 late thymocyte development. *Nat Immunol* 10: 840-847.
707 57. Johnson, A. L., L. Aravind, N. Shulzhenko, A. Morgun, S. Y. Choi, T. L. Crockford, T. Lambe,
708 H. Domaschenz, E. M. Kucharska, L. Zheng, C. G. Vinuesa, M. J. Lenardo, C. C. Goodnow, R. J.
709 Cornall, and R. H. Schwartz. 2009. Themis is a member of a new metazoan gene family and is
710 required for the completion of thymocyte positive selection. *Nat Immunol* 10: 831-839.
711 58. Wang, D., M. Zheng, L. Lei, J. Ji, Y. Yao, Y. Qiu, L. Ma, J. Lou, C. Ouyang, X. Zhang, Y. He, J.
712 Chi, L. Wang, Y. Kuang, J. Wang, X. Cao, and L. Lu. 2012. Tespa1 is involved in late thymocyte
713 development through the regulation of TCR-mediated signaling. *Nat Immunol* 13: 560-568.
714 59. Li, Q. J., J. Chau, P. J. Ebert, G. Sylvester, H. Min, G. Liu, R. Braich, M. Manoharan, J. Soutschek,
715 P. Skare, L. O. Klein, M. M. Davis, and C. Z. Chen. 2007. miR-181a is an intrinsic modulator of
716 T cell sensitivity and selection. *Cell* 129: 147-161.
717
718
719
720
721
722
723
724
725

Footnotes

This work was supported by the Fondation ARC pour la recherche sur le cancer (C.M.), La Ligue contre le cancer (C.M.), Fondation Pasteur Mutualite (C.M.), Nancy Taylor Foundation for Chronic Disease (E.M.B.) and NIH grants R03 AI097611 (J.M.J.), R01 HL112836 (E.M.B.), R01 AI121250-A1 (E.M.B.), R21 A1 135435 (C.H.B.), and RO1 AI 112621 (C.H.B.).

734 **Figure Legends**
735
736
737 **Figure 1.** *PG* mice exhibit impaired thymocyte developmental transitions that require TCR gene
738 assembly. **(A)** Representative flow cytometry plots of DN stages of thymocyte development showing the
739 frequency of cells at each stage. **(B)** Quantification of numbers of cells in each DN stage. **(C)**
740 Representative flow cytometry plots of DN, DP, $CD4^+$ SP, and $CD8^+$ SP thymocytes. **(D)** Quantification
741 of numbers of cells in each stage. **(E)** Quantification of the ratio of $CD4^+$ SP or $CD8^+$ SP thymocytes to
742 DP thymocytes. **(F-G)** Quantification of the numbers of total thymocytes (F) and splenic αβ T cells (G).
743 (A-G) All data were collected from 6-10 weeks old mice and (B, D, E, F, and G) are combined from four
744 independent experiments including a total of 14-16 mice per genotype. Bars indicate mean +/- SEM. Stats:
745 2-way ANOVA with Sidak multiple comparison test. n.s. $p>0.05$; * $p<0.05$, **$p<0.01$, *** $p<0.001$, ****
746 $p<0.0001$.
747
748 **Figure 2.** Thymocytes of *PG* mice support diminished levels of *Tcrb* and *Tcra* recombination. **(A-B)**
749 Taqman qPCR quantification of rearrangements of each Vβ segment to DJβ1.1 (A) or DJβ2.1 (B)
750 complexes conducted on genomic DNA from DN3 thymocytes. Signals from each assay were normalized
751 to values from an assay for the invariant CD19 gene. Shown are average values +/- SEM from three
752 independent DN cell preparations. **(C)** Adaptive Immunoseq quantification of the percentage usage of
753 each Vβ in *Tcrb* rearrangements of DN3 thymocytes. Shown are average values from two independent
754 DN cell preparations. **(D)** qPCR quantification of specific Vα/Jα rearrangements peformed on genomic
755 DNA from DP thymocytes. Signals from each assay were normalized to values from an assay for the
756 invariant β2m gene. Shown are the average values +/- SEM from three independent DP cell preparations.
757 For all graphs in figure: #, not detected, n.s. $p>0.05$; * $p<0.05$, **$p<0.01$, *** $p<0.001$, **** $p<0.0001$
758

759 **Figure 3.** Thymocytes of *PG* mice have reduced Syk and Zap70 protein levels. **(A-B)** Representative flow
760 cytometry histogram plots (A) and quantification (B) of Syk protein in DN3 thymocytes. (B) Shown are
761 all data points and average values +/- SEM from one of two independent experiments (n = 3-4 mice per
762 genotype, unpaired t-test). **(C)** qRT-PCR quantification of Syk mRNA in DN3 cells. Relative mRNA
763 levels were calculated using ddCt method with signals from each assay normalized to values from an assay
764 for the *Hprt* gene. Shown are all data points and average values +/- SEM from two independent
765 experiments (n = 8-9 mice per genotype, 2-way ANOVA with experiment an independent variable, stats
766 indicate difference as a result of genotype). **(D)** Gating strategy for Stages 1-4 of DP thymocyte selection.
767 Pre-gated on live singlets and $CD8^+$ and/or $CD4^+$. **(E-H)** Representative flow cytometry histogram plots
768 (E, G) and quantification (F, H) of Zap70 (E, F) and TCRβ (G, H) protein in Stages 1-4 of DP thymocyte
769 selection. (F, H) Shown are all data points and average values +/- SEM from one of three independent
770 experiments (n = 4-5 mice per genotype, 2-way ANOVA with Sidak's multiple comparison post-test) **(I)**
771 qRT-PCR quantification of Zap70 mRNA in DN3 cells or Stage 2 or 4 DP cells. Relative mRNA levels
772 were calculated using ddCt method with signals from each assay normalized to values from an assay for
773 the Hprt gene. Shown are all data points and average values +/- SEM from one experiment (n = 4-5 mice
774 per genotype, 2-way ANOVA with sidak multiple comparison post-test. **(J-K)** Representative flow
775 cytometry histogram plots (J) and quantification (K) of Zap70 protein in naïve $CD4^+$ or $CD8^+$ T cells.
776 Shown are all data points and average values +/- SEM from two independent experiments (n = 3 mice per
777 genotype, 2-way ANOVA with Sidak multiple comparison post-test). For all graphs in figure: n.s. $p>0.05$;
778 * $p<0.05$, ** $p<0.01$, *** $p<0.001$, **** $p<0.0001$.
779
780 **Figure 4.** *PG* mice exhibit impaired positive and negative selection. **(A)** Gating strategy for measuring
781 positive selection of thymocytes showing Stage 1 and 2 gates. Pre-gated on live singlets and $CD4^+$ and/or
782 $CD8^+$. **(B)** Quantification of the ratio of the number of Stage 2 cells to the total number of Stage 1 and 2
783 cells. Shown are all data points and global mean from three independent experiments (n = 10-11 mice per

784 genotype, 2-way ANOVA indicating effect of genotype). **(C)** Gating strategy form measuring negative
785 selection of Vβ6$^+$ and Vβ8$^+$ thymocytes in F1 progeny of C57BL/6 background *PG* mice bred with
786 BALB/c background *Rag1*$^{-/-}$ mice. Pre-gated on live singlets. **(D)** Quantification of ratios of indicated Vβ$^+$
787 cells that progress to post-selection versus those Vβ$^+$ cells that are produced at the pre-selection stage.
788 Normalized to total thymocytes in pre or post-selection population and *WT* controls. Shown are all data
789 points and average +/- SEM from two independent experiments (n = 9 mice per genotype, 2-way ANOVA
790 with Sidak multiple comparison post-test. For all graphs in figure: n.s. $p>0.05$; * $p<0.05$, ** $p<0.01$, ***
791 $p<0.001$, **** $p<0.0001$.
792
793
794 **Figure 5.** Mature αβ T cells of PG mice exhibit normal immune response. **(A)** Representative plot of
795 cytokine expression on CD4$^+$CD44^{hi} αβ T cells following *ex vivo* stimulation of splenocytes with PMA
796 and ionomycin. **(B-F)** Representative analyses of naïve splenic CD4$^+$ or CD8$^+$ T cells after *ex vivo*
797 simulation with anti-CD3/anti-CD28 antibodies and additional antibodies to skew towards indicated
798 lineages. Shown is CFSE incorporation (B) or expression of relevant transcription factors (C, D) or
799 cytokines (E, F). **(G, H)** Representative flow data showing (G) frequencies of splenic αβ T cells that stain
800 with the gp33:H-2Db tetramer or (H) express indicated cytokines after LCMV infection of mice. Data are
801 representative of two independent experiments with at least four mice of each genotype. **(I, J)**
802 Representative plots (J) and (I) quantification of antigen-specific αβ T cells able to respond to indicated
803 viral peptides within a peptide re-stimulation assay. (A-F) Data are representative of two independent
804 experiments. (G-J) Data are combined from four independent experiments (two D7 and two D35
805 timepoints) with 8-11 mice of each genotype per time-point.
806
807

808 **Figure 6. Mat**ure αβ T cells of *PG* mice possess higher than normal autoimmune hazard**. (A)** Graph of
809 body weights of *Rag1*$^{-/-}$ hosts over time after transfer of *WT* or *PG* CD4^{+} T cells or no cells (NT). Data
810 combined from three independent experiments with a total of 13-17 mice of each genotype. Lines indicate
811 fitted segmented-linear regression lines +/- 95% confidence interval. Day 15 was fixed as the inflection
812 point. Difference between gradients of second slope was determined by linear regression analysis. **(B)**
813 Numbers of CD4^{+} T cells in spleen eight weeks post-transfer. **(C)** Total number of IFNγ, TNFα, and/or
814 GM-CSF producing cells per spleen. Shown are all data points from three independent experiments with
815 12-14 mice per group. Bar indicates global mean. Pre-gating on live singlets, CD90.2^{+}, CD4^{+}, and CD44^{+}.
816 **(D)** Colon length of mice sacrificed at eight weeks post-infection. **(E)** Representative hemotoxylin and
817 eosin stained colon sections from respective mice at eitght weeks post-transfer. 10x magnification. **(F-G)**
818 Total colitis score as assessed by blinded pathologist. Scored as per previously described guidelines for
819 the five phenotypes (44): (F) Colon inflammation score (contribution of scores for crypt abcesses and
820 inflammatory cell infiltrate). (G) Colon tissue damage score (contribition of scores for crypt architecture,
821 tissue damage, goblet cell loss). **(H)** Non-colitis pathologies described for mice transferred with *WT* versus
822 *PG* cells. **(I)** Hemotoxylin and eosin stained skin section from *PG*-transferred mouse with severe
823 dermatitis at eight weeks post-transfer. 10x magnification. **(J)** Spleen weight at eight weeks post-transfer
824 normalized to total mouse bodyweight prior to transfer. **(K)** Survival curves of mice transferred with *WT*
825 or *PG* cells. Data combined from three independent experiments. Statistical analysis = Log-rank Mantel-
826 Cox test. Overall: 0/13 NT mice died, 1/15 *WT*-transferred mice died, and 4/17 *PG*-transferred mice died.
827 (B, C, F, G, and J) Shown are all data points from three independent experiments, 12-14 mice per group.
828 Experiment indicated by shape of data point. Bar indicates global mean. Analyzed by 2-way ANOVA
829 with Tukey HSD post-test. n.s. $p>0.05$; * $p<0.05$, ** $p<0.01$, *** $p<0.001$, **** $p<0.0001$ (**L**) Curves
830 showing diabetes free survival of female NOD *WT* and *PG* mice. Mice were generated by mating together
831 NOD *Rag1*$^{WT/PG}$ mice and monitored for their first 30 weeks of life. The percent diabetes survival curves

include mice that have passed 20 weeks of age or gotten diabetes before 20 weeks of age. Analyzed by Gehan-Breslow-Wilcoxon test. p=0.049.

857 **Figure 1**

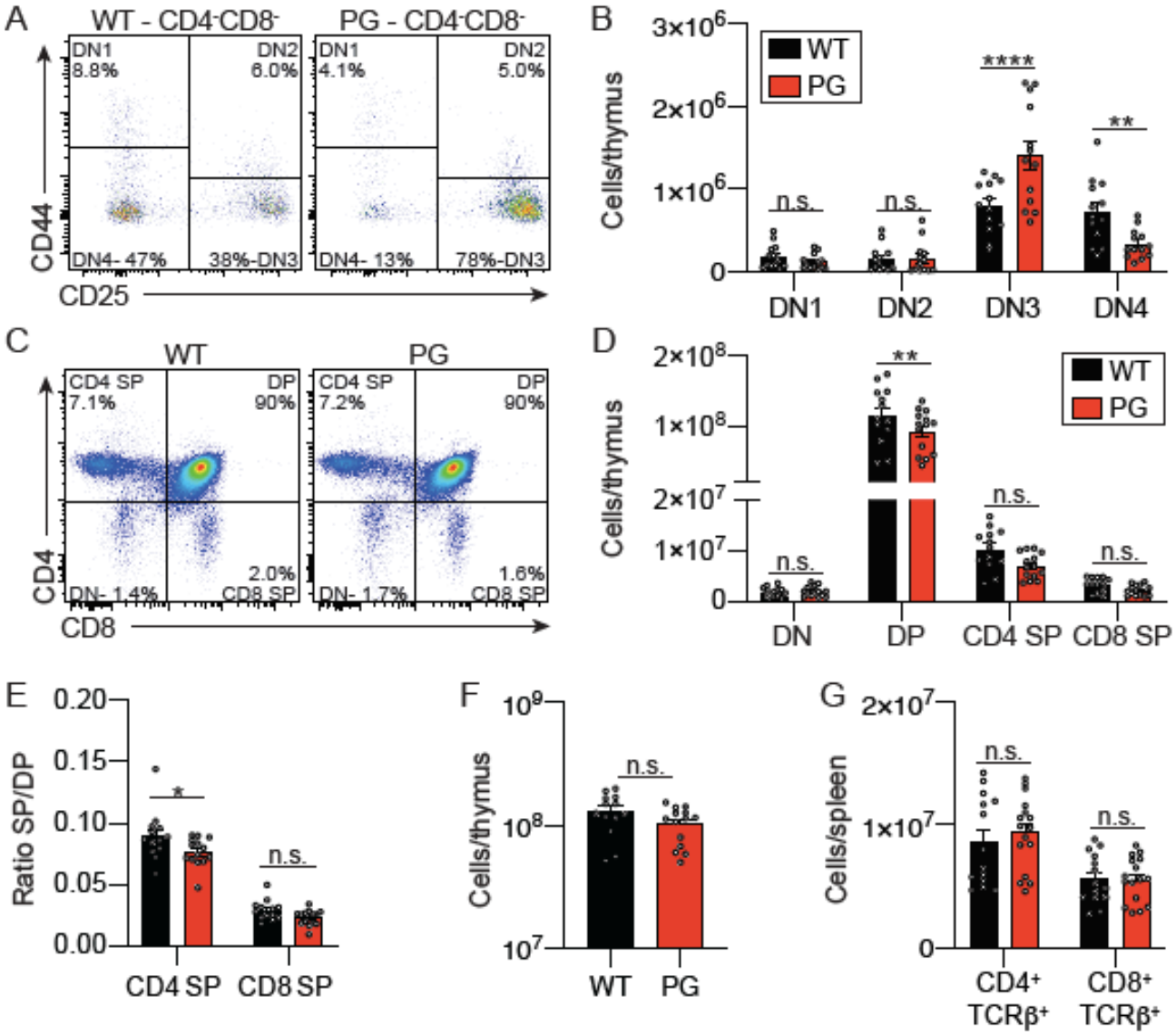

858

859

860

861

862

863

864

865

866 **Figure 2**

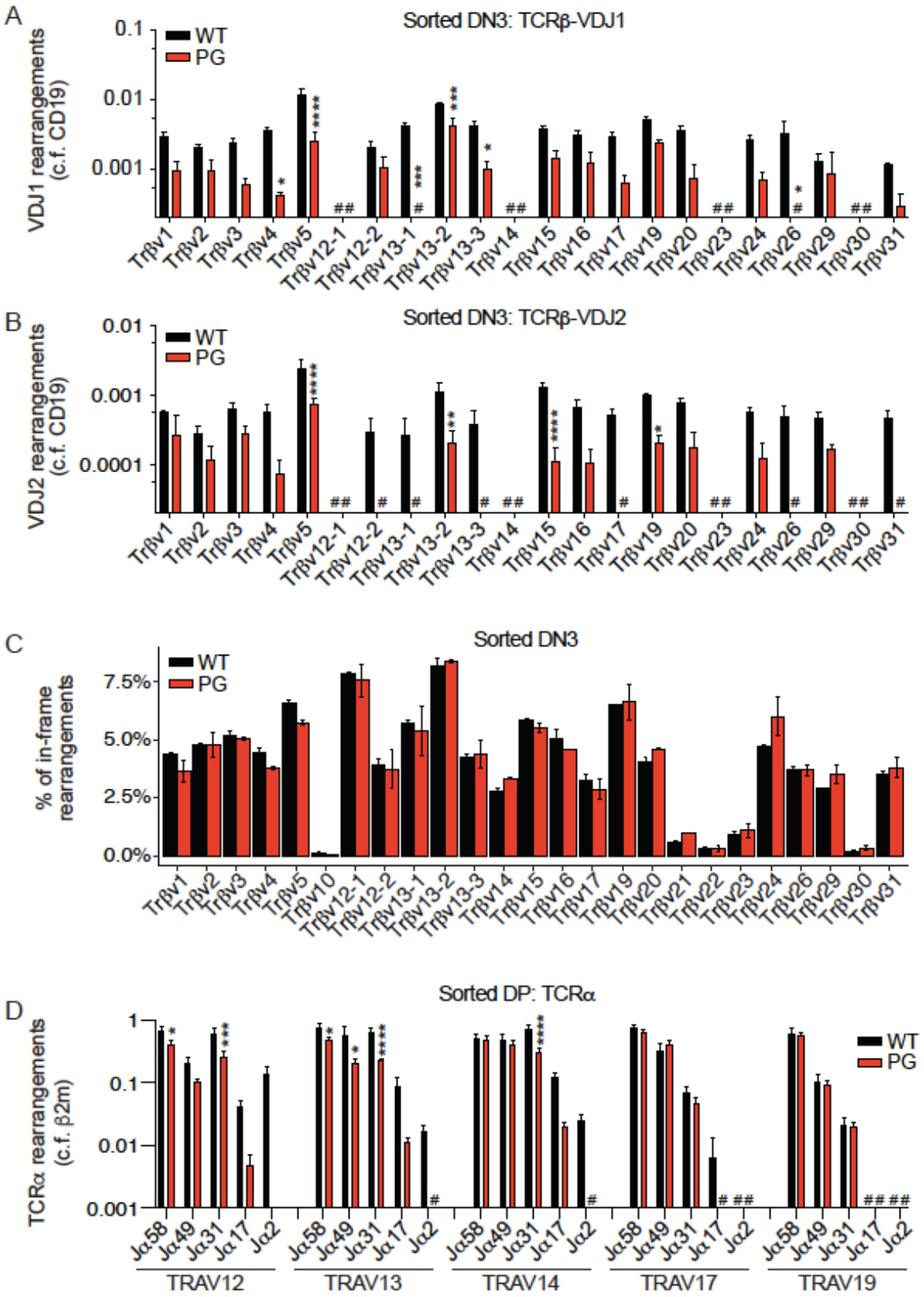

867

868 **Figure 3**

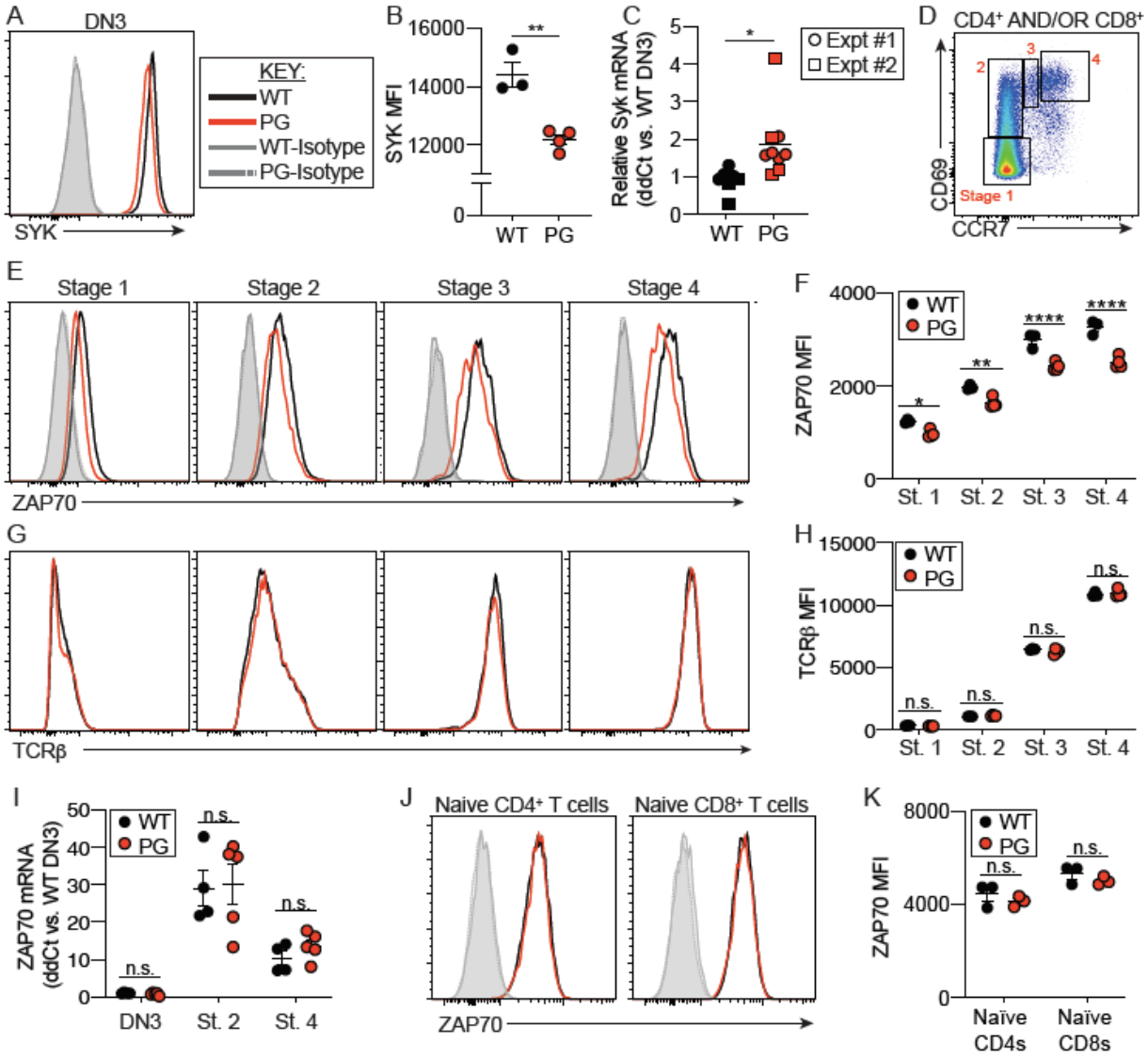

869

870

871

872

873

874

875

876

877 **Figure 4**

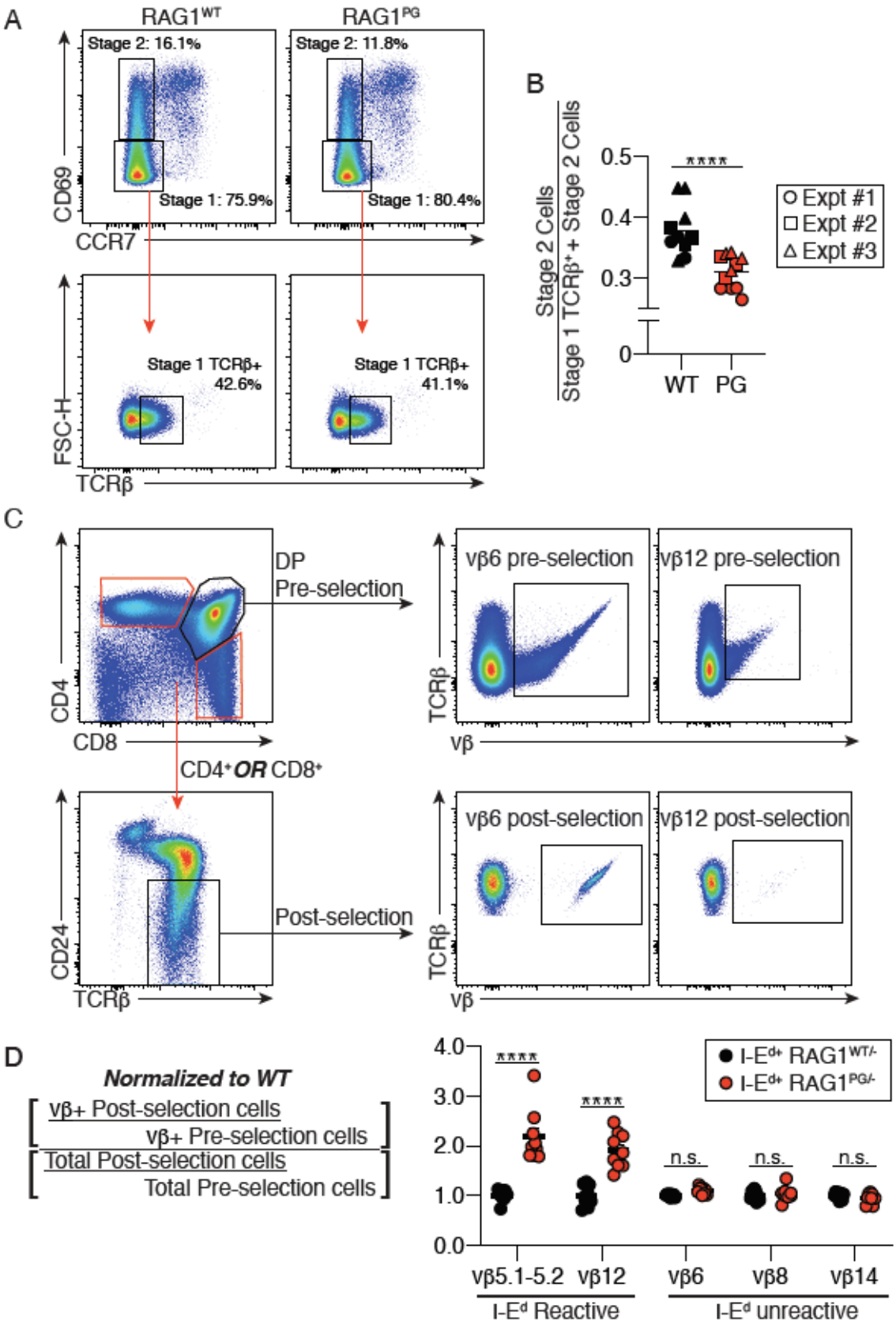

878

879
880 **Figure 5**
881

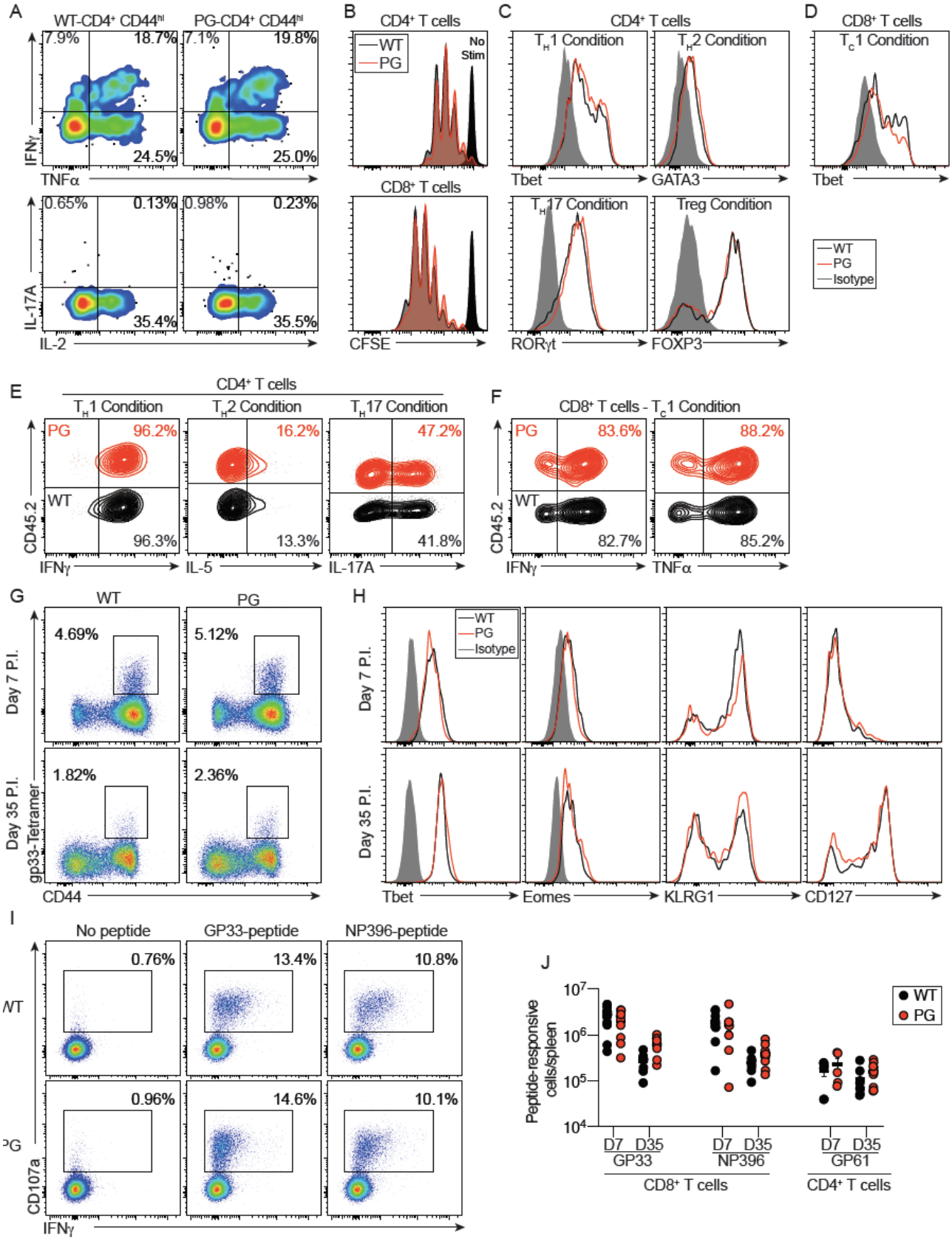

882

Figure 6

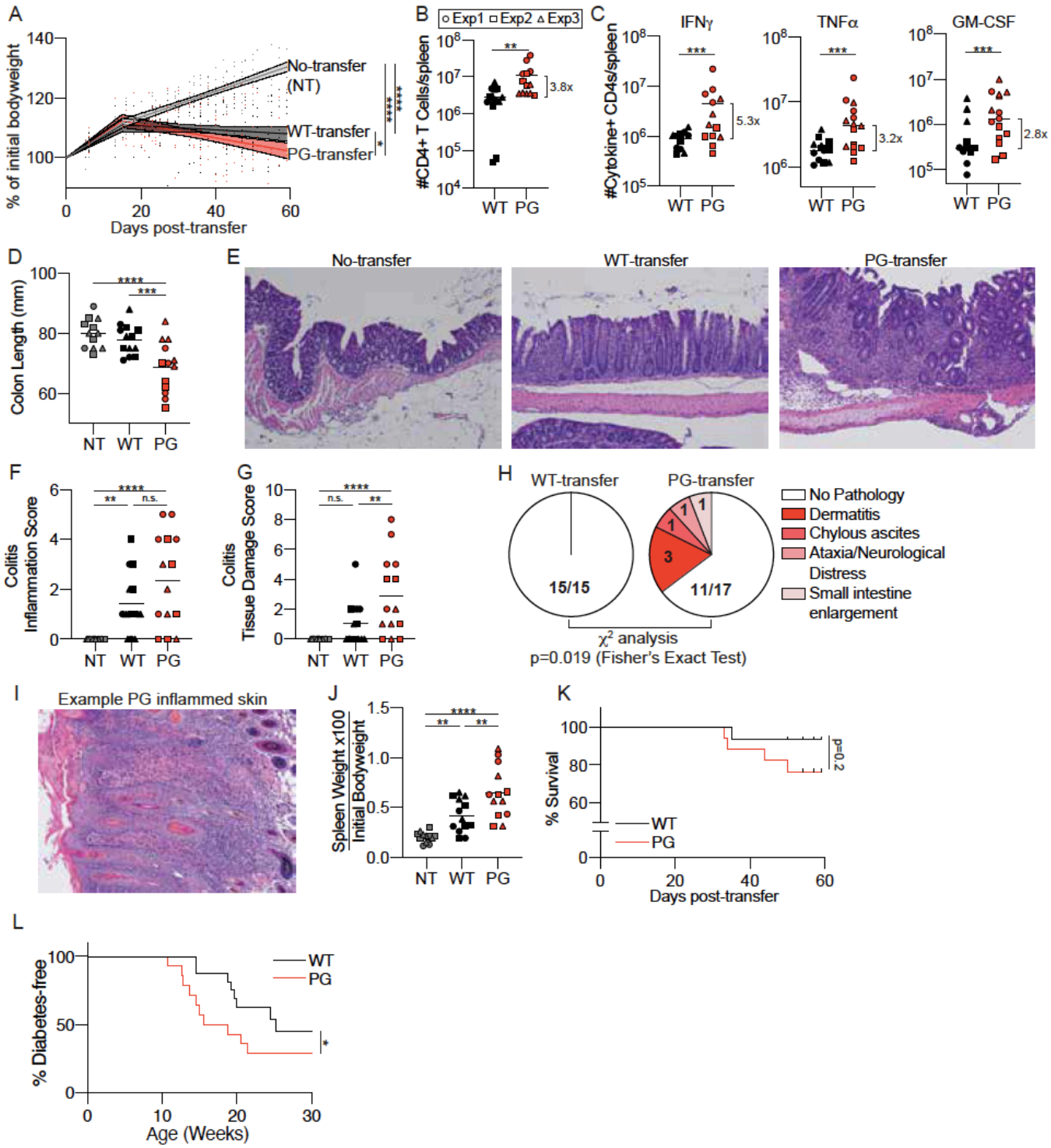
A
% of initial bodyweight
Days post-transfer
No-transfer (NT)
WT-transfer
PG-transfer
B
Exp1 Exp2 Exp3
#CD4+ T Cells/spleen
3.8x
C
IFNγ
TNFα
GM-CSF
#Cytokine+ CD4s/spleen
5.3x
3.2x
2.8x
WT PG
D
Colon Length (mm)
NT WT PG
E
No-transfer
WT-transfer
PG-transfer
F
Colitis Inflammation Score
G
Colitis Tissue Damage Score
H
WT-transfer
PG-transfer
15/15
11/17
No Pathology
Dermatitis
Chylous ascites
Ataxia/Neurological Distress
Small intestine enlargement
χ² analysis
p=0.019 (Fisher's Exact Test)
I
Example PG inflammed skin
J
Spleen Weight x100 / Initial Bodyweight
K
% Survival
p=0.2
L
% Diabetes-free
Age (Weeks)